Hybrid Microgrid With Parallel- and Series-Connected Microconverters

Jinwei He, *Member, IEEE*, Yunwei Li, *Senior Member, IEEE*, Chengshan Wang, *Senior Member, IEEE*, Yiwei Pan, Chenghui Zhang, *Member, IEEE*, and Xiangyang Xing, *Student Member, IEEE*

***Abstract*—In this paper, a hybrid microgrid with series- and parallel-connected microconverters is proposed. A few series-connected low voltage microconverters are used to build a string converter with rated output voltage magnitude. Then, the parallel operation of string converters increases the power rating and redundancy of the microgrid. To realize both grid-tied and islanding microgrid control with proper power sharing, a hierarchical power regulation method is developed with simultaneous point of common coupling (PCC) voltage and microconverter voltage control. First, the well-understood droop control is adopted to obtain PCC voltage reference for power sharing between parallel string converters. Second, a power balancing regulation through microconverter local voltage control is used to redistribute output power demand among series-connected microconverters in a string converter. As the string converter line current measured by all microconverters is the same, it is utilized to develop a novel synchronizer to interconnect the string converter central controller and the microconverter local controllers with only low bandwidth communications. Due to the coordination of string converter central control and microconverter local control, the proposed hybrid microgrid can operate in grid-tied and islanding modes with real and reactive power sharing for each microconverter.**

***Index Terms*—Decentralized control, droop control, hierarchical control, hybrid microgrid, low bandwidth communication (LBC), power control.**

I. Introduction

THE growing installation of distributed generation (DG) units has brought structural changes to modern power distribution systems. When multiple parallel DG units are operating together, they can form a microgrid to provide more flexible power supply to the loads within the power distribution network [1].

Manuscript received July 14, 2016; revised October 27, 2016 and January 17, 2017; accepted March 13, 2017. Date of publication April 24, 2017; date of current version February 22, 2018. Recommended for publication by Associate Editor Li Zhang. *(Corresponding author: Jinwei He.)*

J. He and C. Wang are with the School of Electrical and Information Engineering, Tianjin University, Tianjin 300072, China (e-mail: 18202539408@163.com; cswang@tju.edu.cn).

Y. Li is with the Department of Electrical and Computer Engineering, University of Alberta, Edmonton, AB T6G 2R3, Canada (e-mail: yunwei.li@ualberta.ca).

Y. Pan, C. Zhang, and X. Xing are with the School of Control Science and Engineering, Shandong University, Ji'nan 250000, China (e-mail: cinsdllpyv@163.com; zchui@sdu.edu.cn; xxy198513@163.com).

Color versions of one or more of the figures in this paper are available online at http://ieeexplore.ieee.org.

Digital Object Identifier 10.1109/TPEL.2017.2695659

An important feature of microgrid is the capability of islanding operation [2]–[4], where proper power sharing should be achieved between parallel DG units. The master-slave control can be adopted to regulate the system. However, this control method has a few limitations, such as the use of high bandwidth communication to transmit the instantaneous voltage references to each DG unit slave controller. Accordingly, this method can reduce system reliability and may cause poor dynamic performance during load transients [8]. To avoid the use of high bandwidth communications, the well-understood droop control method [5] for the operation of distributed synchronous generators [17] has been utilized for controlling parallel DG units. Nevertheless, the conventional droop control may cause stability problems and reactive power sharing errors, particularly when the microgrid system has imbalanced/harmonic loads [6], [7] or feeder is mainly resistive [9]. In recent literature, many modified methods have been developed to improve the performance of droop control. For instance, the virtual real and reactive power [10] and the virtual frequency and voltage magnitude [11] concepts have been proposed to decouple the real and reactive power sharing control. To maintain a stable operation of weak microgrid and to improve the reactive power sharing control accuracy, the virtual impedance based control method was proposed in [2], [12], and [13]. More recently, the hierarchical control has been applied to control a microgrid or a microgrid cluster. With the help of this control algorithm, ac system frequency, point of common coupling (PCC) voltage magnitude, and dc rail voltage deviations can be fully compensated at steady-state, through either centralized secondary control [14], [15] or distributed secondary control [16]. Note that in this process, to compensate the difference between power demand and the available power from the back stage renewable energy resources, the battery or super capacitor system can be included in the dc links of the droop-controlled DG unit [22], [23].

Due to the continued progress of multilevel converter techniques, a DG unit often has a few low voltage (LV) converter modules with multiple energy sources [18]. The cascaded H-bridge or modular multilevel converter topologies are the most well-known interfacing converter candidates. However, previous research is mainly focused on the output power and current response of the interfacing converter. In this situation, the internal power demand allocation among LV cells can hardly be achieved. To address this problem, a few enhanced control methods have been proposed to have better management of internal

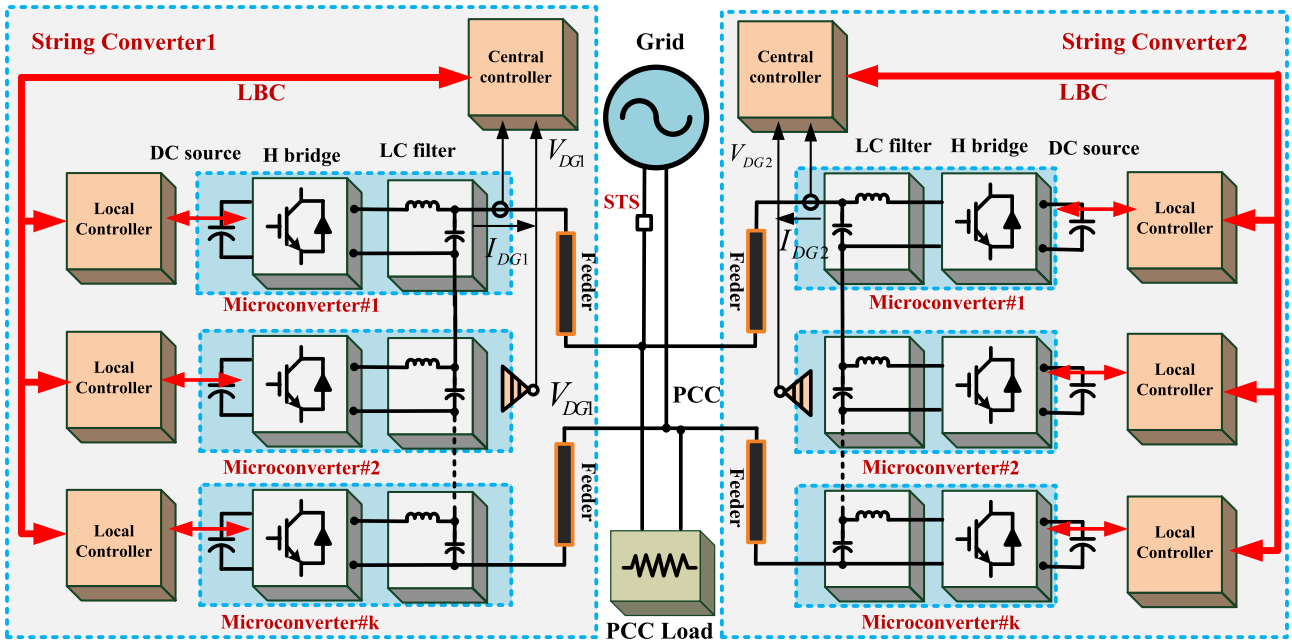

Fig. 1. Diagram of a parallel- and series-connected microconverters based hybrid microgrid.

power allocation of the system [19]. In [20] and [21], the real and reactive power reference of each H-bridge cell is designed to have independent maximum power point tracking or optimal reactive power support. In addition to single-phase applications, the power quality issues of this topology in a three-phase system, such as the interphase imbalance current compensation, were discussed in [30].

In recent year, the series-connected LV microconverters with an *LC* filter for each cell are used to build up a DG interfacing converter [24]–[26]. It has been verified in [24] and [33] that these new topologies can provide more flexibility and reduce the cost of grid-tied converters. First, the high voltage dc wiring is not needed due to the use of only LV dc rails. Second, the high set-up dc/dc boost converter for the conventional DG unit in [18] is removed from the system. To promote the applications of series microconverters based DG-grid interfacing converters in a dual-mode microgrid, some topics should be further discussed:

1) Due to the limitation of renewable energy resources availability, remotely installed microconverters are often connected in series as a string converter system. In this case, long distance high bandwidth communications between microconverters and microgrid central control can reduce the reliability of the system.
2) Previous research in [24] and [25] mainly focused on the operation in grid-tied mode. For dual-mode microgrid applications, the voltage support scheme for islanding microgrid should be developed.
3) Conventional droop control methods do not have the capability to regulate the power sharing between series-connected LV converter modules. To solve this limitation, the inverse power factor droop control in [26] has been applied to maintain power sharing between series-connected converters in islanded system.

Unfortunately, the output characteristics of this DG unit are not compatible with other DG units regulated by conventional droop control. Therefore, developing a generalized power control method that can realize proper power sharing at both DG unit string converter level and microconverter cell level is definitely needed.

Motivated by the above-mentioned discussions, series- and parallel-connected microconverters are used to form a microgrid with both grid-tied and islanding operation capability. First, a few series-connected microconverters are used to form a string converter. Then, the parallel-connection of string converters is used to supply power to the microgrid. The proposed system uses a hierarchical power sharing scheme where the upper control scheme is responsible for power sharing between parallel string converters and the lower level control is responsible for distributing the power demand among series-connected microconverters. With this control algorithm, the system can be more flexible as each microconverter is able to participate in the power sharing in both grid-tied and islanding modes. In order to reduce the burden of communications for hierarchical control, the fundamental component of string converter line current is utilized as a synchronizer to form a novel synchronizer between string converter central control system and microconverter local control system. Simulated and experimental results verify the correctness of the proposed system.

II. Proposed Hybrid Microgrid

Fig. 1 shows the configuration of the proposed hybrid microgrid. The system is composed of two parallel DG units. Each DG unit is interfaced to PCC with a string converter. The PCC of the microgrid is then connected to the main grid with static transfer switch (STS). When the main grid is not available, the

STS is OFF and the system operates in autonomous islanding mode. In this case, the PCC load should be powered up by the parallel string converters.

The power circuit of a string converter is composed of a few series-connected microconverters. Each microconverter has an *LC* output filter. These microconverters work together to get a suitable string converter output voltage magnitude for grid integration. The central controller regulates the output power and voltage of the string converter. It is also connected with microconverter local controllers with low bandwidth communications (LBCs). The local controller of the microconverter regulates the output voltage of the microconverter for power balancing control between series microconverters.

A. DG Unit Power Control

For grid-connected operation, the DG-grid interfacing string converter can inject controllable real and reactive power into the main grid. First, by using LBC links, the string converter central controller receives the information of all microconverters. For instance, the information of state of charge of the back stage battery banks or the dc voltage of the super capacitors can be collected by the DG unit central controller. Then, the real power reference $P_{\rm ref}$ and the reactive power reference $Q_{\rm ref}$ of the string converter are determined by the preset energy management strategies [22]. With the above-mentioned power management mechanism, the output power reference of microconverter k can be re-expressed as

$$P_{{\rm ref},\,k} = \varepsilon_{p,\,k} P_{\rm ref} \tag{1}$$

$$Q_{{\rm ref},\,k} = \varepsilon_{q,\,k} Q_{\rm ref} \tag{2}$$

where $P_{{\rm ref},k}$ and $Q_{{\rm ref},k}$ are the reference real and reactive power of microconverter k. The coefficients $\varepsilon_{p,k}$ and $\varepsilon_{q,k}$ are the output power ratio of microconverter k in this string converter.

To have a closed-loop control of the string converter output power, the droop control can be implemented in string converter central controller as

$$\omega_{\rm DG} = \omega^* + D_p \cdot \frac{\omega_{\rm cut}}{s+\omega_{\rm cut}} \cdot (P_{\rm ref} - P_{\rm DG}) \tag{3}$$

$$E_{\rm DG} = E^* + \left(D_q + \frac{k_{\rm iq}}{s}\right) \cdot \frac{\omega_{\rm cut}}{s+\omega_{\rm cut}} \cdot (Q_{\rm ref} - Q_{\rm DG}) \tag{4}$$

where ω^* and $\omega_{\rm DG}$ are the nominal and the reference angular frequencies of the string converter. E^* and $E_{\rm DG}$ are the nominal and reference string converter voltage magnitudes. $P_{\rm DG}$ and $Q_{\rm DG}$ are the string converter real and reactive power measured by the central controller. $\omega_{\rm cut}$ is the cut-off frequency of low bandwidth filters D_P, D_q, and $k_{\rm iq}$ are coefficients of the power loop controller. It is necessary to note that the integral control in (4) can ensure zero steady-state reactive power tracking error for string converter grid-tied operation. As the output reactive power is determined by the PCC load demand in islanding operation mode, this gain k_{iq} should be set to zero for parallel string converters power sharing when the main grid is OFF.

When the voltage magnitude and frequency references are determined by (3) and (4), the instantaneous voltage reference

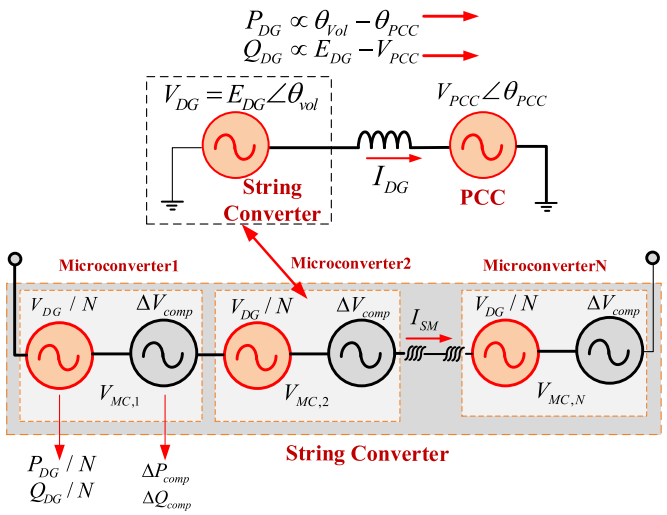

Fig. 2. Equivalent circuit of a string converter system.

$V^*_{{\rm DG},\,C}$ can be obtained by using a reference generator as

$$V^*_{{\rm DG},\,C} = E_{\rm DG} \sin\left(\int \omega_{\rm DG}\, dt\right). \tag{5}$$

It is necessary to note that with the regulation of string converter output voltage as $V^*_{{\rm DG},\,C}$, it can be self-synchronized with the main grid without using any phase-locked-loops (PLLs). This is similar to the characteristics of the "synchronverters" as discussed in [31].

B. Microconverter Local Power Control

With the controllers in (1)–(5), the output power of a string converter system can be effectively regulated. The output power of a string converter is the sum of the output power of all series-connected microconverters. Nevertheless, the power reference ratio of each microconverter has not been determined yet.

Assuming all series microconverters in a string converter equally share the output power command, the reference voltage in (5) can be divided by the series-connected microconverter numbers N. Then, it is used as the reference voltage for all microconverters as

$$V^*_{{\rm MC},\,k} = V^*_{{\rm DG},\,L}/N \tag{6}$$

where $V^*_{{\rm MC},\,k}$ is the reference voltage of microconverter k and $V^*_{{\rm DG},\,L}$ is the string converter voltage reference received by the microconverter local controller. The method of transmitting the reference voltage $V^*_{{\rm DG},\,C}$ from the string converter central controller to microconverter local controllers as $V^*_{{\rm DG},\,L}$ will be discussed later in the next section.

Note that the output power of these microconverters can be different for better power management of a string converter [22], but the controller in (6) cannot provide this independent power regulation function. This limitation is solved by using a power compensator in the microconverter local controller, as shown in Figs. 2 and 3.

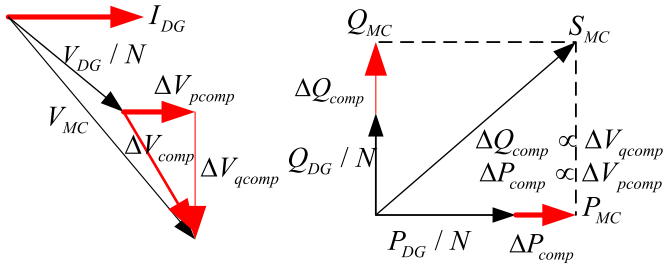

Fig. 3. Phasor diagram of a microconverter.

First, the equivalent circuit of a string converter is shown in Fig. 2. As shown in the top half of the figure, the string converter is modeled as a controlled voltage source, where the real power flow $P_{\rm DG}$ is in proportion to the phase angle difference between string converter output and PCC voltages as $\theta_{\rm Vol} - \theta_{\rm PCC}$ and the reactive power flow $Q_{\rm DG}$ is in proportion to the voltage magnitude difference as $E_{\rm DG} - V_{\rm PCC}$.

The equivalent circuit of a string converter is composed of a few series-connected LV-controlled voltage sources. For each microconverter, it is represented by two voltage sources as $V_{\rm DG}/N$ and $\Delta V_{\rm comp}$ as shown in the lower part of Fig. 2. When only $V_{\rm DG}/N$ is working and $\Delta V_{\rm comp}$ is zero, the real and reactive power command is equally shared by all series microconverters. But when $\Delta V_{\rm comp}$ is not zero, this term can be used to actively adjust the microconverter output power as $\Delta P_{\rm comp}$ and $\Delta Q_{\rm comp}$, according to the power control requirement.

The relationship between a microconverter output power variations and the corresponding voltage term $\Delta V_{\rm comp}$ is shown in Fig. 3. The reference frame is aligned to the string converter line current phasor. It can be seen that when there are some changes of microconverter voltage, the variation of real power $\Delta P_{\rm comp}$ is in proportion to voltage phasor $\Delta V_{p\rm comp}$ in the horizontal direction and the change of reactive power $\Delta Q_{\rm comp}$ is in proportion to the voltage phasor $\Delta V_{q\rm comp}$ that is 90 degree lagging of the line current.

According to this relationship, the closed-loop local power control of a microconverter k is given as

$$\begin{aligned} V^*_{{\rm MC},k} &= V^*_{{\rm DG},L}/N + \Delta V_{p\rm comp} + \Delta V_{q\rm comp} \\ \Delta V_{p\rm comp} &= \left(k_{p,\rm MC} + \frac{k_{i,\rm MC}}{s}\right)(\varepsilon_{p,k} P_{\rm DG} - P_{{\rm MC},k}) \\ &\quad \times \cos\left(\theta_{{\rm Cur},L}\right) \\ \Delta V_{q\rm comp} &= \left(k_{p,\,\rm MC} + \frac{k_{i,\,\rm MC}}{s}\right)(\varepsilon_{q,\,k} Q_{\rm DG} - Q_{{\rm MC},\,k}) \\ &\quad \times \sin\left(\theta_{{\rm Cur},\,L}\right) \end{aligned} \tag{7}$$

where $k_{p,\,\rm MC}$ is the proportional gain and $k_{i,\,\rm MC}$ is the integral gain of the PI regulator for independent microconverter local real and reactive power regulation and $\theta_{{\rm Cur},\,L}$ is phase angle of the string converter line current detected by the microconverter local controller.

When the reference voltage for microconverter k is determined, the well-understood double-loop voltage controller as shown in [5] is selected for fast microconverter voltage tracking. The outer control loop is given as

$$\begin{aligned} I^*_{{\rm ref},\,k} &= G_{\rm Outer}(s) \cdot \left(V^*_{{\rm MC},\,k} - V_{C,\,k}\right) \\ &= \left(k_p + \frac{2k_i\omega_c s}{s^2 + 2\omega_c s + \omega^{*2}}\right) \cdot \left(V^*_{{\rm MC},\,k} - V_{C,\,k}\right) \end{aligned} \tag{8}$$

where $V_{C,\,k}$ is the measured microconverter LC filter capacitor voltage, k_p is the proportional gain, k_i is the gain of the quasi-resonant controller, and ω_c is the cut-off frequency of the quasi-resonant controller.

The inner control loop for microconverter output current tracking is given as

$$\begin{aligned} V^*_{{\rm PWM},\,k} &= G_{\rm Inner}(s) \cdot \left(I^*_{{\rm ref},\,k} - I_{o,\,k}\right) \\ &= k_{\rm Inner} \cdot \left(I^*_{{\rm ref},\,k} - I_{o,\,k}\right) \end{aligned} \tag{9}$$

where $I^*_{{\rm ref},\,k}$ is reference current of the inner current control loop, $I_{o,\,k}$ is the output current of the microconverter, $k_{\rm Inner}$ is the inner loop proportional gain, and $V^*_{{\rm PWM},\,k}$ is the reference voltage of the H-bridge based microconverter k.

III. String Converter and Microconverter Coordination

In the previous section, the information of the string converter, including the string converter real and reactive power ($P_{\rm DG}$ and $Q_{\rm DG}$), the output power ratio reference ($\varepsilon_{p,\,k}$ and $\varepsilon_{q,\,k}$) of each microconverter and the instantaneous reference voltage ($V^*_{{\rm DG},\,C}$), shall be sent from the string converter central controller to microconverter local controllers. It is important to note that the instantaneous voltage reference ($V^*_{{\rm DG},\,C}$) is an ac quantity. Thus, it is difficult to send this information via the conventional LBC systems.

To overcome this limitation, a novel communication method using the fundamental string converter line current as a synchronizer is proposed, as shown in Fig. 4. First, the magnitude and phase angle of the reference voltage $V^*_{{\rm DG},\,C}$ and the phase angle of line current $I_{{\rm DG},C}$ are obtained via the sliding discrete Fourier transform (DFT) [27] at the string-converter central controller as $E_{{\rm DG},C}$, $\theta_{{\rm Vol},C}$, and $\theta_{{\rm Cur},\,C}$. The sliding DFT here is a fast calculation scheme that can obtain phase angle and magnitude of signals at fundamental and harmonic frequencies using only sampled data of one fundamental cycle.

For steady-state reference voltage, the magnitude of reference voltage $E_{{\rm DG},C}$ is dc. In addition, it can be seen that the power regulation using droop control usually has slow dynamics. Accordingly, the difference of voltage and current phase angle $\Delta\theta_C = \theta_{{\rm Vol},\,C} - \theta_{{\rm Cur},\,C}$ is also dc quantity for small time-scale analysis. This means the dynamic response of $\Delta\theta_C$ is slow and it can only change in a small range in a few switching cycles [15]. In this case, these two dc components $E_{{\rm DG},\,C}$ and $\Delta\theta_C$ can be sent from the string converter central controller to the microconverter local controllers via an LBC. It is necessary to note that the detection of reference voltage and line current phase angle using sliding DFT is only for the synchronization of central controller and local controller using LBCs. It is not the same as grid-synchronization using PLLs [32].

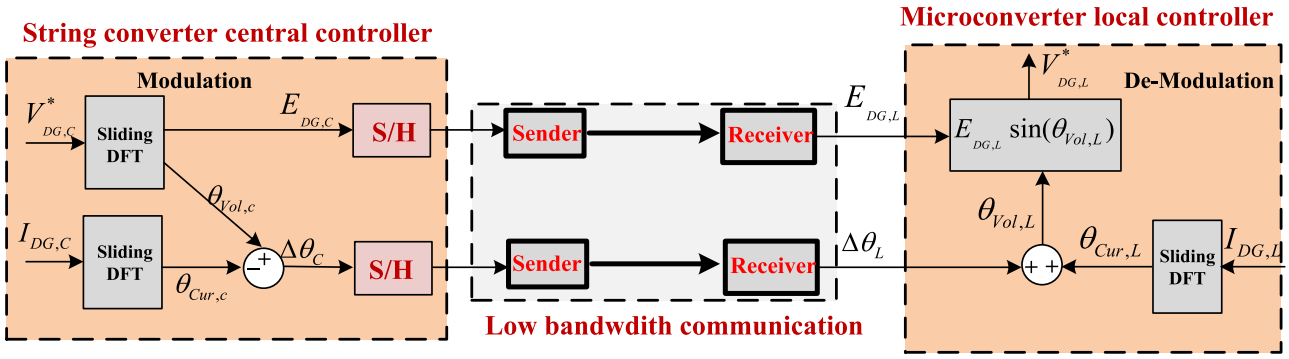

Fig. 4. Low-bandwidth communication between string converter central controller and microconverter local controller.

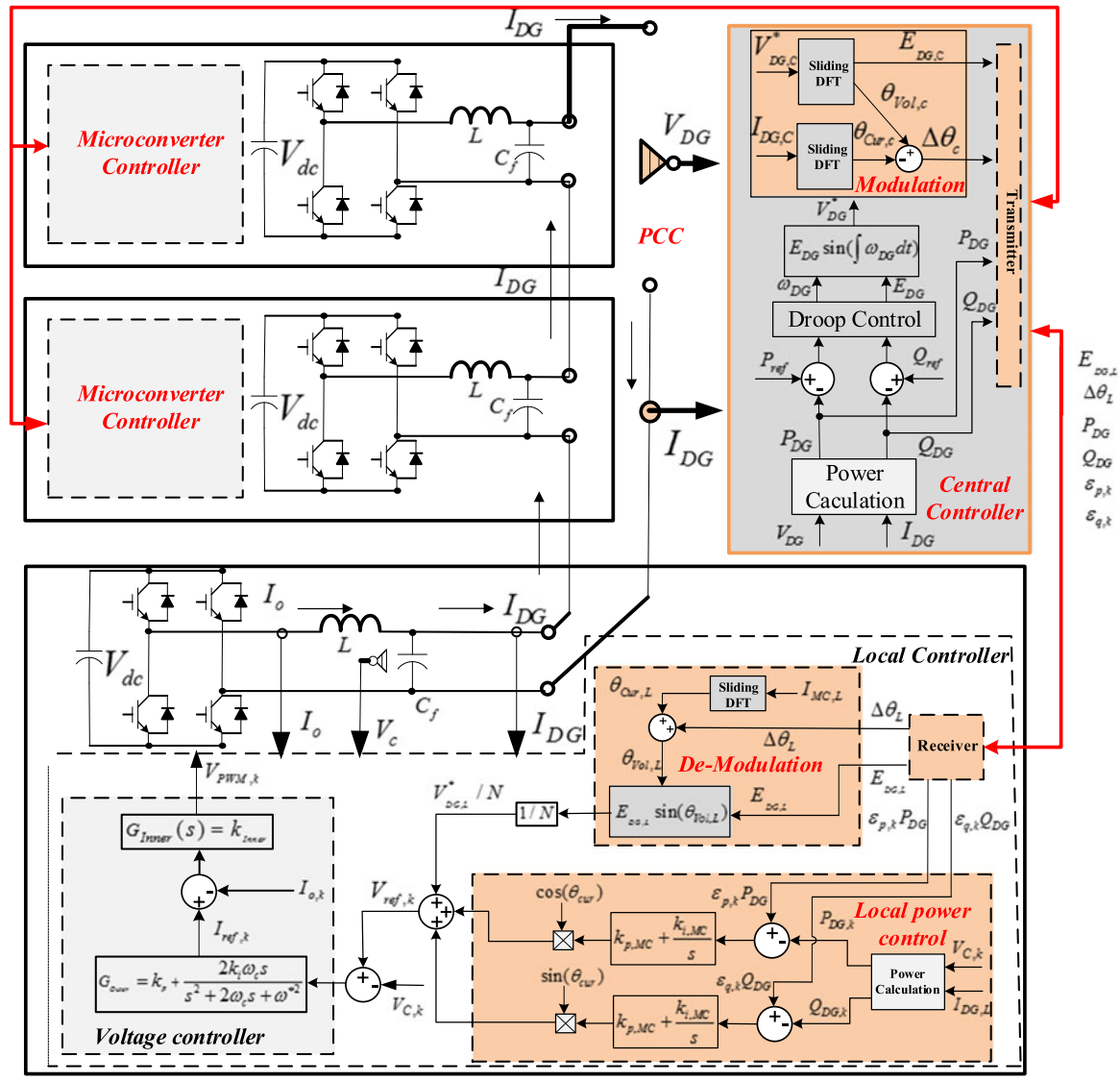

Fig. 5 . Control diagram for a string converter system.

Due to the feature of series-connected configuration, the central controller and the microconverter local controller measure the same string converter current as I_{DG}. With this finding, the received signals $E_{\mathrm{DG},\,L}$ and $\Delta\theta_L$ at microconverter local controller can be used to reconstruct the instantaneous reference voltage as

$$V^{*}_{\mathrm{DG},\,L} = E_{\mathrm{DG},\,L}\sin\left(\Delta\theta_L + \theta_{\mathrm{Cur},\,L}\right) \tag{10}$$

where $V^{*}_{\mathrm{DG},L}$ is string converter instantaneous reference voltage obtained by the microconvetrer local controller, $E_{\mathrm{DG},L}$ and

TABLE I
PARAMETERS OF THE SIMULATED AND EXPERIMENTAL SYSTEM

Circuit Parameter	Value
Grid voltage	Single-phase 120 V/50 Hz
Microconverter numbers in a string converter	4
Microconverter *LC* filter	$L_1 = 1$ mH $R_1 = 8$ mΩ; $C_f = 60\ \mu$F;
DC link voltage	165 V
Switching frequency	20 kHz
PCC *RL* load	$R = 10\,\Omega$ $L = 25$ mH
Feeder impedance	String Converter1: $R = 0.2\,\Omega$, $L = 1.7$ mH String Converter2: $R = 0.2\,\Omega$, $L = 2.0$ mH
Central Controller parameter	Value
Real power droop coefficient	$D_P = 1/550$
Reactive power droop coefficient	$D_q = 1/220$ $k_{\mathrm{iq}} = 1/45$
Sampling frequency for SDFT	20 kHz
Local Controller parameter	Value
Sampling frequency for SDFT	20 kHz
Power control coefficient	$k_{P,\mathrm{MC}} = 1/100$, $k_{i,\mathrm{MC}} = 1/70$
Outer loop control	$k_p = 0.1$, $k_i = 20$, $\omega_c = 5$ rad/s
Inner loop control	$k_{\mathrm{inner}} = 20$

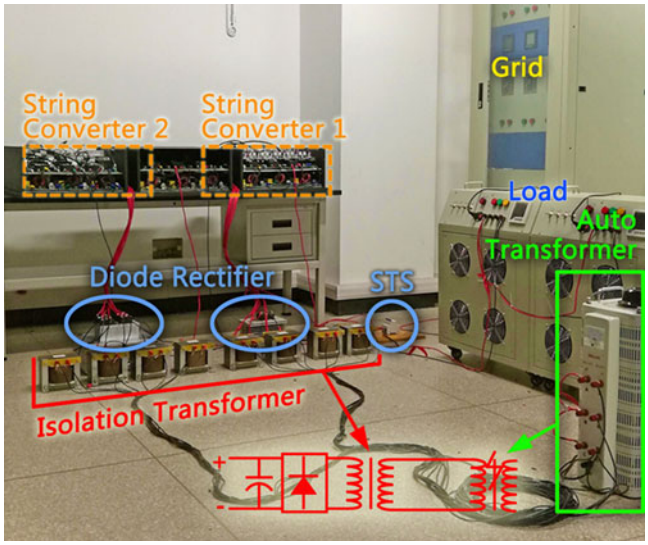

Fig. 6. Experimental prototype.

$\Delta\theta_L$ are the reference voltage magnitude and the phase angle difference obtained by microconverter. Similarly, $\Delta\theta_{\mathrm{Cur},\,L}$ is the string converter line current phase angle obtained by microconverter local measurements. Then, the instantaneous reference voltage for a microconverter can be obtained as shown in (10). When both the central controller control scheme and the local controller control scheme are introduced, the complete control diagram of the string converter system can be seen in Fig. 5.

IV. VERIFICATION RESULTS

To verify the performance of the proposed system, simulated and experimental results are provided in this section. The parameters of the system can be seen in Table I. The experimental prototype with two string converters is shown in Fig. 6, where each microconverter is constructed by insulated gate bipolar transistors (IGBTs) from Infineon. Both the central and the local control schemes are developed on TI TMS320 F 28335 DSP boards. The dc links are powered up by diode rectifiers with isolation transformer placed at the front end.

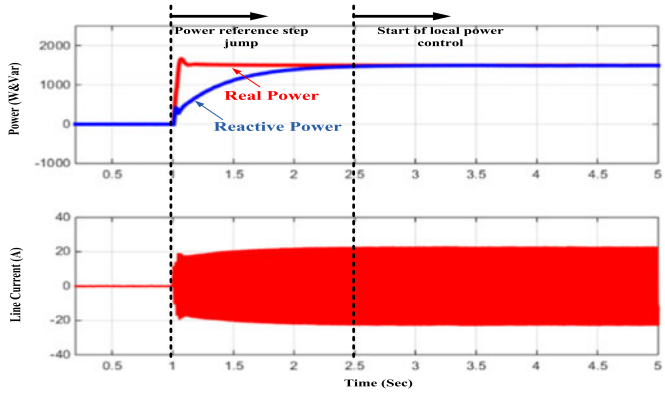

Fig. 7. String converter power control performance (*Grid-tied*).

A. Simulation

The simulation is conducted in the MATLAB/Simulink environment. The configuration of the system is the same as that in Fig. 1.

1) Grid-Tied Operation: First, the grid-tied operation of a string converter is verified. When the real and reactive power references are set to 1500 W and 1500 Var at 1.0 s, the dynamic performance of the system is shown in Fig. 7. For the sake of simplicity, the dc links of the microconverters are connected to four isolated dc sources at 135 V. In addition, the LBC system is emulated by a zero-order hold with only 300 Hz sampling frequency.

Similar to the performance of a conventional droop control based DG unit, it can be seen from Fig. 7 that the real power response is fast while the reactive power dynamic response is relatively slow. The corresponding string converter current is shown in the lower half of the figure. Note that there are some enhanced methods, such as the adaptive virtual impedance control and the feed-forward voltage control [12] to improve the reactive power tracking performance. However, a further discussion is out of the scope of this paper.

The performance of each microconverter is also investigated. In the beginning of the simulation, the microconverter local power control is not activated and four microconverters have the same voltage reference. Accordingly, they equally share the power command as shown in Figs. 8 and 9. When the power control command ratio for microconverters are set to $\varepsilon_{p,1} = 0.325$, $\varepsilon_{p,2} = 0.275$, $\varepsilon_{p,3} = 0.225$, $\varepsilon_{p,4} = 0.175$, $\varepsilon_{q,1} = 0.175$, $\varepsilon_{q,2} = 0.225$, $\varepsilon_{q,3} = 0.275$, and $\varepsilon_{q,4} = 0.325$ at 2.5 s, it can be seen that all microconverter output power slowly reaches the command value at the steady-state.

When the local power control is implemented in the microconverter local controller, the line current waveform of the string converter is shown in Fig. 10. It can be clearly seen that there is no obvious overshoot during the start of the local power control.

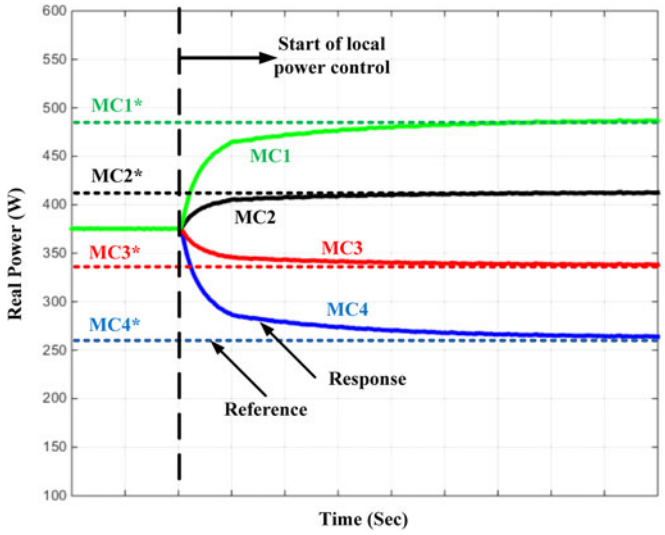

Fig. 8. Microconverters real power control performance (*Grid-tied*).

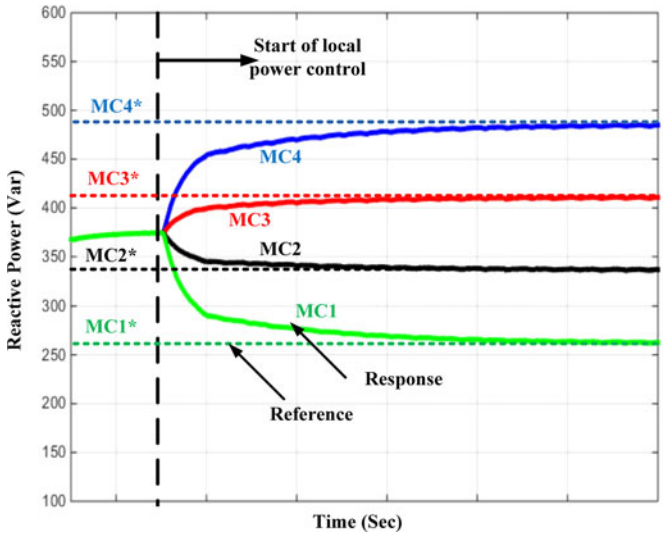

Fig. 9. Microconverters reactive power control performance (*Grid-tied*).

The microconverter voltage waveforms before and after the use of the proposed microconverter local power control are shown in Fig. 11. Without using the proposed local power control method, the voltage waveforms of four microconverters are almost the same. When output powers of four microconverters are not the same due to the activation of local power control, the ac voltage waveforms also have obvious differences.

In order to demonstrate that the proposed method is still effective even when the microconverter dc source voltage has some variations, another simulation was conducted as shown from Figs. 12 to 16. In this test, microconverter1 and microconverter2 dc rails are connected to super capacitors (1F), while other microconverters are connected fixed voltage dc sources. The string converter output power has a ramp increase from 1500 to 3000 W at 4.5 s. The line current and the string con-

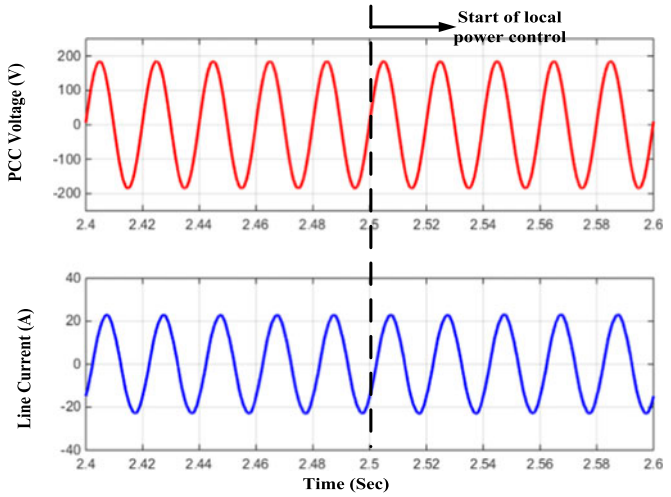

Fig. 10. PCC voltage and string converter line current during the transition of local power regulation (*Grid-tied*).

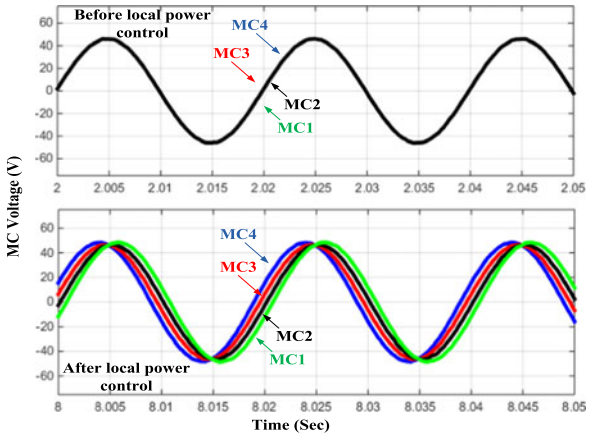

Fig. 11. Microconverter voltage before and after local power control (*Grid-tied*).

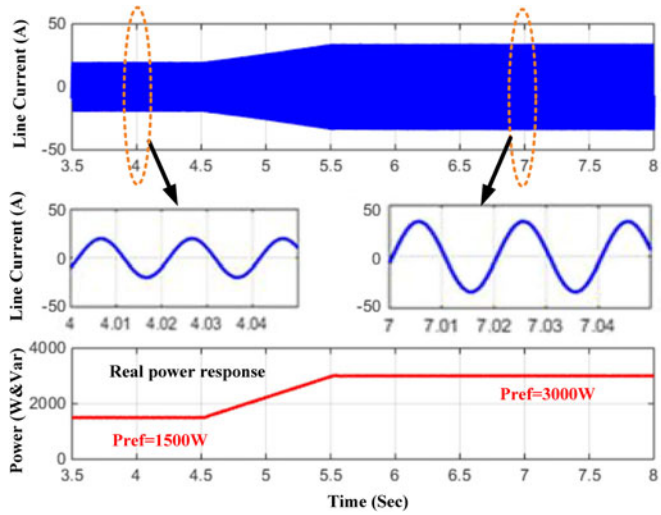

Fig. 12. String converter dynamic performance (*Grid-tied*).

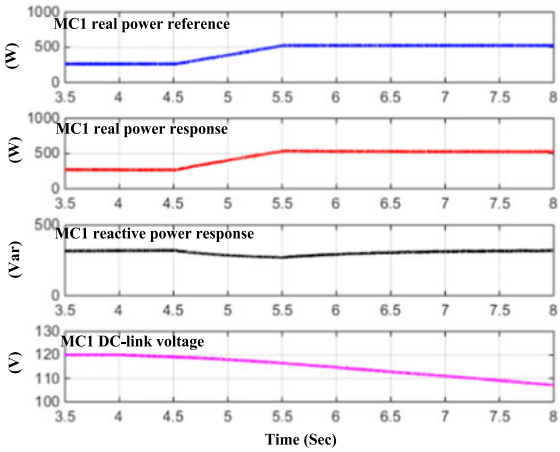

Fig. 13. Microconverter1 dynamic performance (*Grid-tied; dc link connected to super capacitor*).

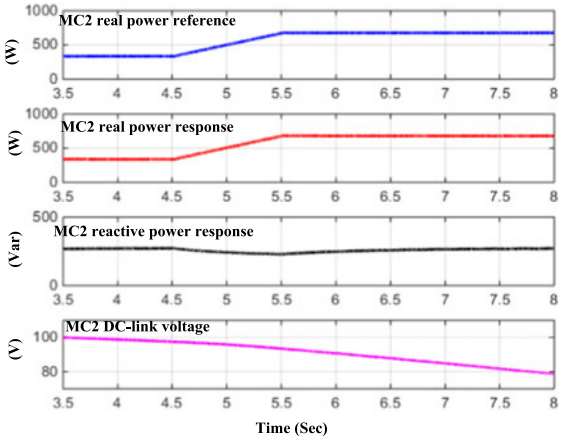

Fig. 14. Microconverter2 dynamic performance (*Grid-tied; dc link connected to super capacitor*).

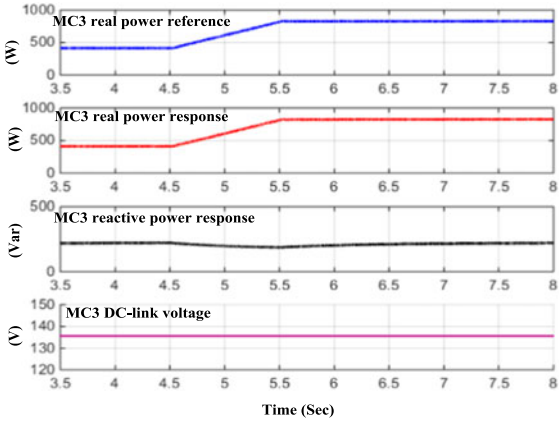

Fig. 15. Microconverter3 dynamic performance (*Grid-tied; dc link connected to ideal voltage sources*).

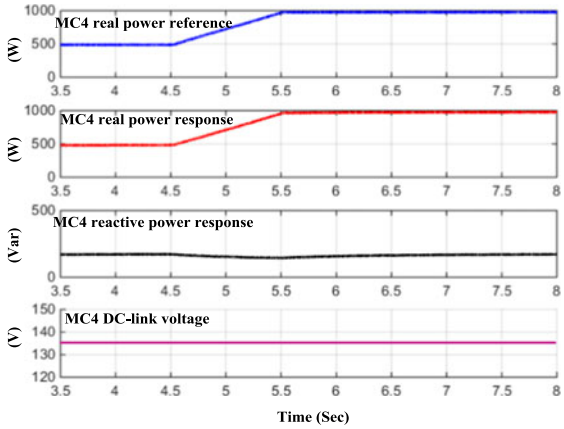

Fig. 16. Microconverter4 dynamic performance (*Grid-tied; dc link connected to ideal voltage sources*).

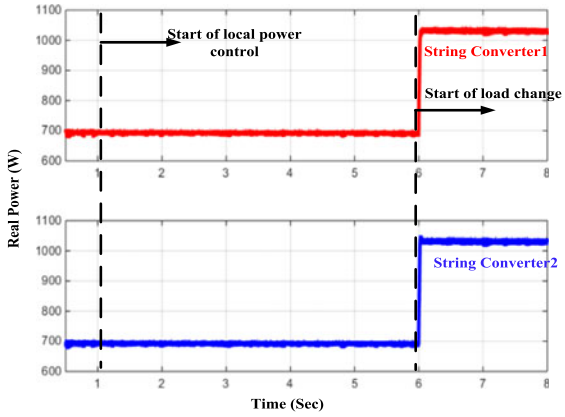

Fig. 17. Two string converters real power sharing performance (*Islanding*).

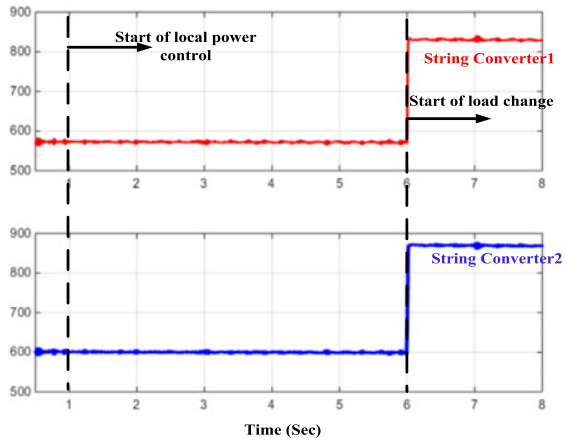

Fig. 18. Two string converters reactive power sharing performance (*Islanding*).

verter output power response in Fig. 12 show that the system can accurately track the power reference and the line current is always sinusoidal before and after the transient.

In addition, the detailed performance of each microconverter in this process is shown from Figs. 13 to 16. As the dc links of microconverter1 and microconverter2 are connected to super capacitor banks, it can be seen from the bottom channels of Figs. 13 and 14 that the dc link voltage of microconverter1 dips from 120 to 108 V and the dc link voltage of microconverter2 dips from 100 to 81 V. Even with some dc voltage variations, the microconverter1 and microconverter2 output real power as shown in the second channel has an accurate tracking of reference in the first channel.

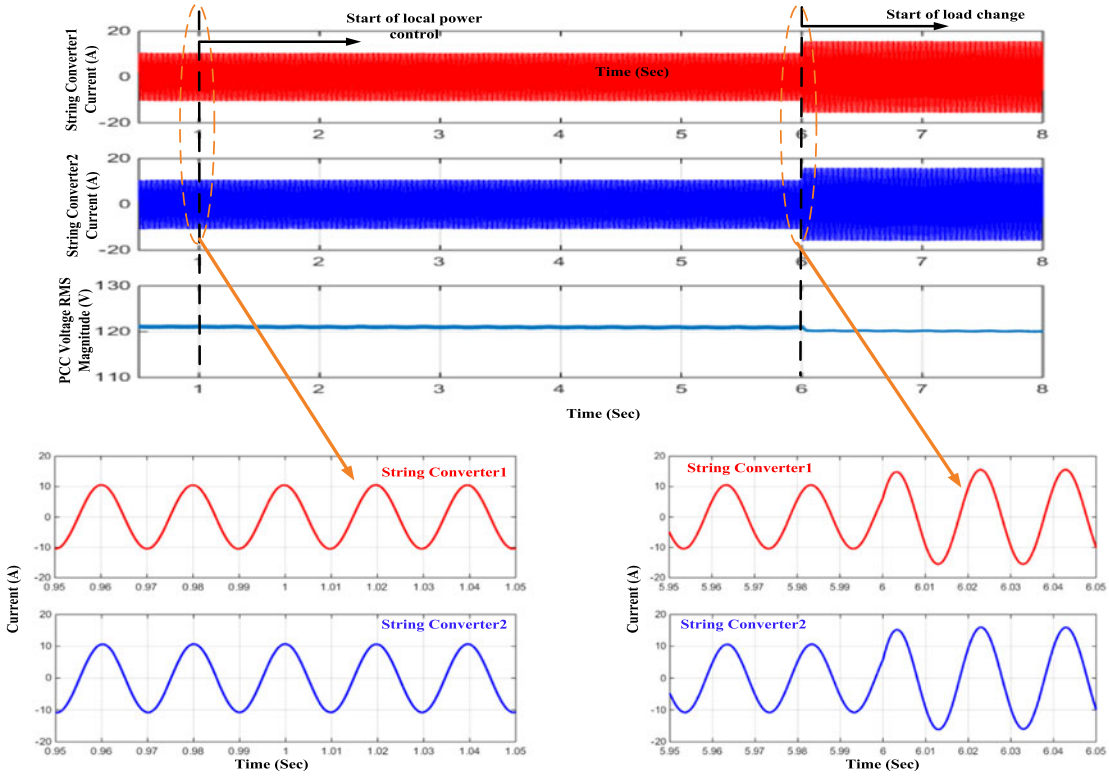

Fig. 19. Two string converters line current and PCC voltage magnitude (*Islanding*).

Note that similar to [28] and [29], the adaptive power management schemes through gain adjustment can be applied to the system to obtain proper management of dc link voltage. Nevertheless, in this system, we intentionally produced mismatched dc voltage variations to verify the correctness of the proposed power control and power redistribution method in adverse situations.

2) Islanding Operation: When the main grid is OFF, parallel string converters can provide continued electricity to PCC loads. The islanding operation of a hybrid microgrid with two parallel-connected string converters at the same power rating is also examined.

Figs. 17 and 18 show the power control of two string converters. The system has a PCC load step change at 6.0 s. From the long time-scale waveforms, it can be seen that parallel string converters almost equally share PCC load demand at both the steady-state and the transient. Due to the effect of unequal string converter feeder impedance, there are around 20 Var reactive power sharing errors between string converter1 and string converter2.

Fig. 19 shows the current of two string converters and the PCC voltage magnitude. As illustrated, the PCC voltage magnitude has around 1 V dip after the load step jump. The zoom-in waveform in the bottom of the figure clearly demonstrates that parallel string converters have similar line current in both the steady-state and the transient during load step change.

The detailed power control performance of microconverters in string converter1 is also provided in Figs. 20 and 21. In this test, the proposed microconverter local power control method is

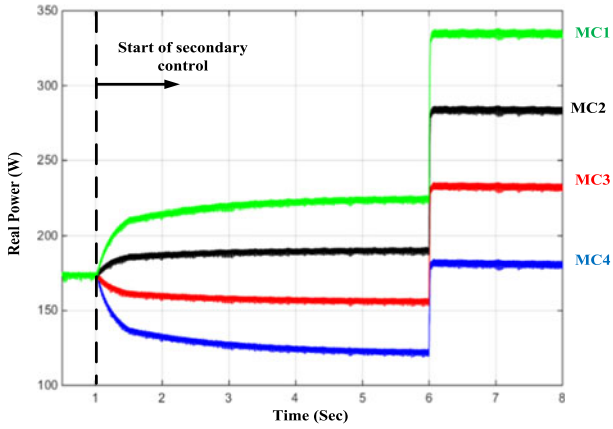

Fig. 20. Microconverters real power control performance (String converter1; *Islanding*).

activated in 1.0 s and the power reference ratios of the microconverters in string converter-1 are $\varepsilon_{p,1} = 0.325$, $\varepsilon_{p,2} = 0.275$, $\varepsilon_{p,3} = 0.225$, $\varepsilon_{p,4} = 0.175$, $\varepsilon_{q,1} = 0.175$, $\varepsilon_{q,2} = 0.225$, $\varepsilon_{q,3} = 0.275$, and $\varepsilon_{q,4} = 0.325$. Accordingly, the output power rapidly drifts to new values after 1 s. When the PCC load has a step change at 6.0 s, each microconverter output power also increases instantly.

It is interesting to find although output power of each microconverter changes according to the PCC load demand variations, the output power ratio for each converter is fixed even during PCC load transient as shown in Figs. 22 and 23.

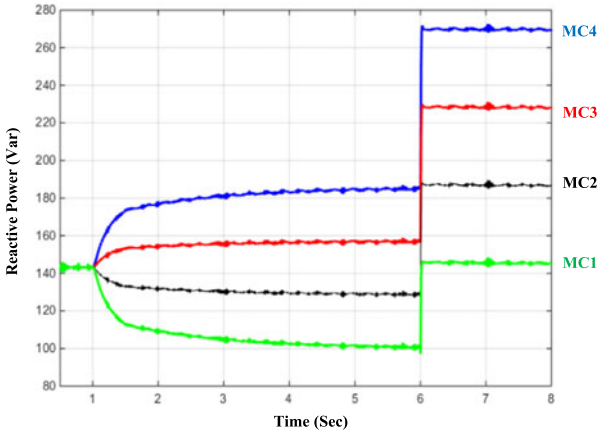

Fig. 21. Microconverters reactive power control performance (String converter1; *Islanding*).

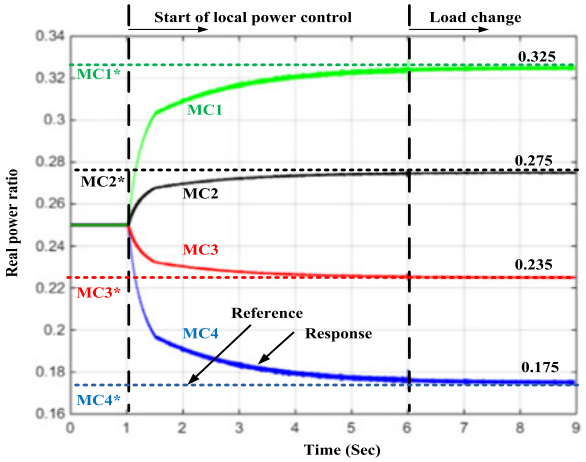

Fig. 22. Microconverters real power ratio (String converter1; *Islanding*).

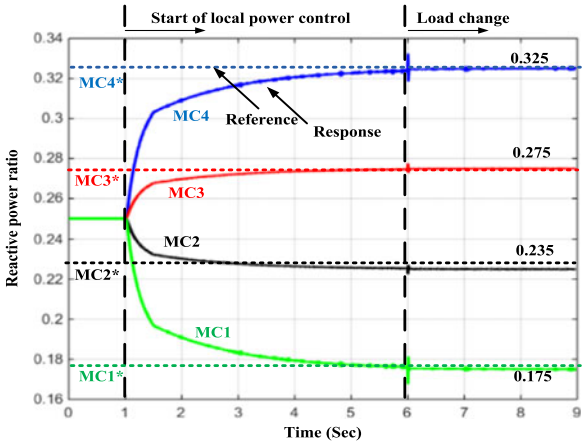

Fig. 23. Microconverters reactive power ratio (String converter1; *Islanding*).

To further demonstrate the performance of the islanding system, the voltage waveform of microconverters in string converter1 is also obtained in Fig. 24. It can be seen that before 1.0 s, four microconverters have similar voltage waveform. When the power commands for microconverters are not the same, the voltages of microconverters are also different due to the use of power regulation term (7) in the local controller.

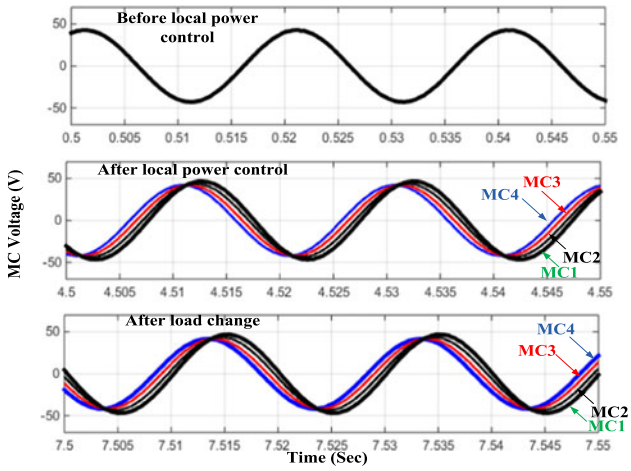

Fig. 24. Microconverters voltage waveforms in various situations (String converter1; *Islanding*).

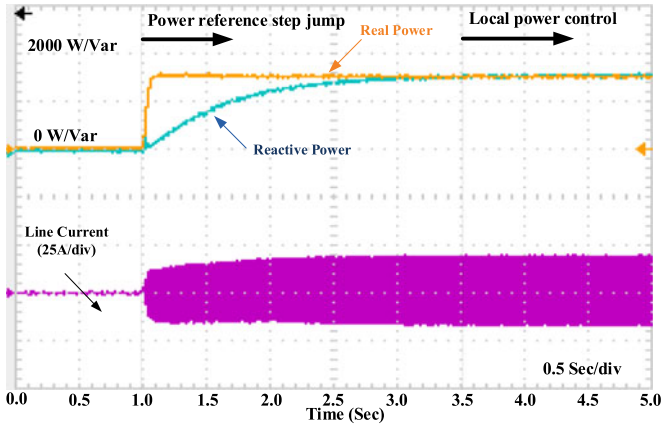

Fig. 25. String converter power control performance (*Grid-tied*).

B. Experiment

Experiments are conducted on a laboratory experimental test rig. The string converter in the test rig has four microconverters connected in series, as shown in Fig. 6. The parameters of the system are shown in Table I. In this experimental system, TI DSP chips at central and local controllers are communicated via RS 485 protocol. The baud rate of the communication protocol is very low at 14 400. In addition, a firm-ware zero-order hold at 250 Hz sampling frequency is implemented at the microconverter local controllers to further verify the effectiveness of the proposed communication method in adverse situations.

1) Grid-Tied Operation: First, the grid-tied operation of a string converter is verified. The string converter is composed of four microconverters. A central controller measures the PCC voltage and the string converter current to get a closed-loop regulation of the output power of the system. In order to emulate the characteristics of LBC in the laboratory test rig, a firmware zero-order hold with 300 Hz sampling frequency is used at

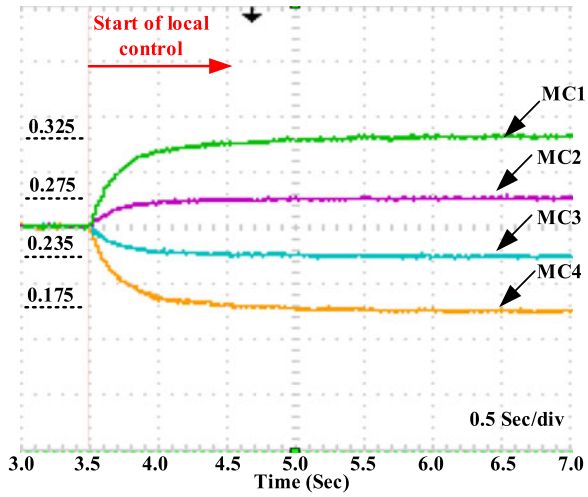

Fig. 26. Microconverters real power control performance (String converter1; *Grid-tied*).

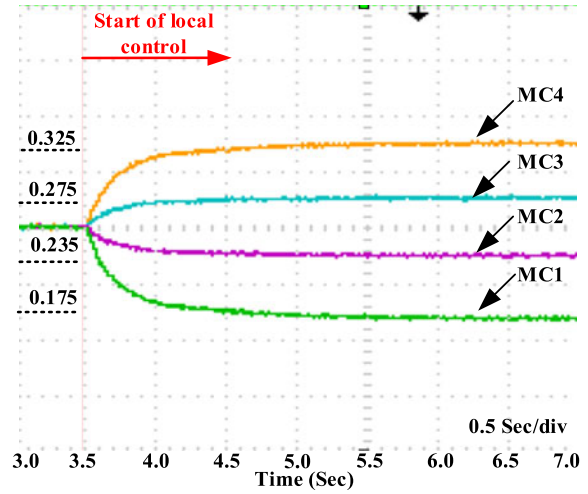

Fig. 27. Microconverters reactive power control performance (String converter1; *Grid-tied*).

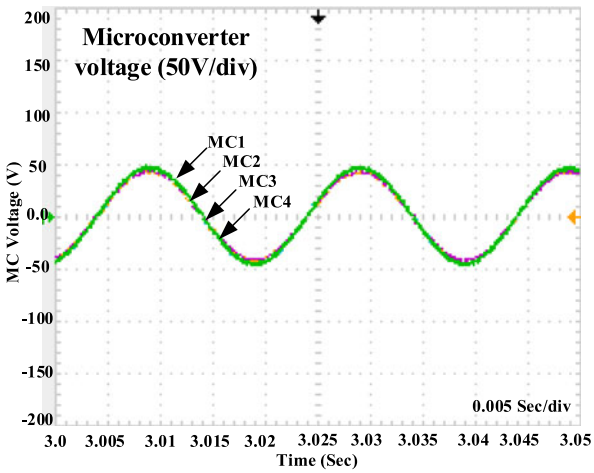

Fig. 28. Microconverters voltage waveforms before local power control (String converter1; *Grid-tied*).

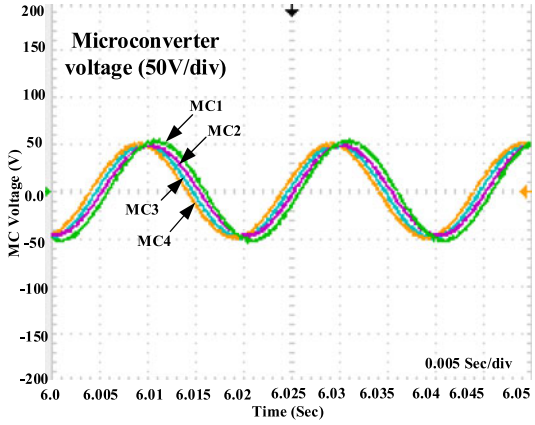

Fig. 29. Microconverters voltage waveforms after local power control (String converter1; *Grid-tied*).

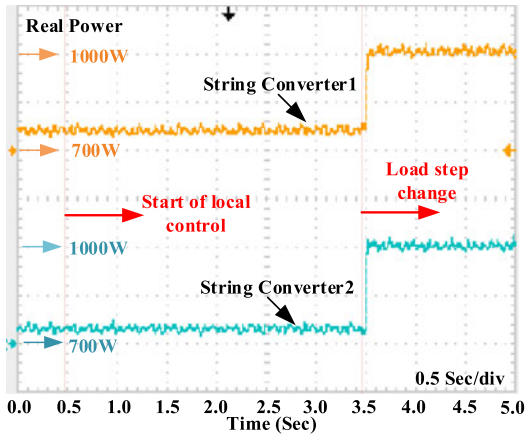

Fig. 30. Two string converters real power sharing performance (*Islanding*).

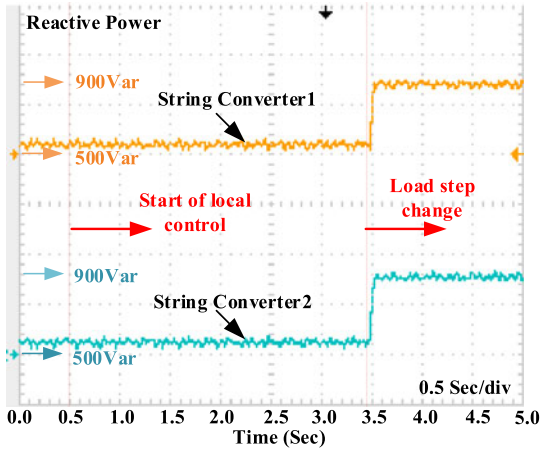

Fig. 31. Two string converters reactive power sharing performance (*Islanding*).

microconverter local controller to reduce the bandwidth of the received signals.

When the real and reactive power references have a step jump from 0 to 1500 W and 0 to 1500 Var at 1.0 s, the dynamic performance of the system is shown in Fig. 25. In addition, the local power control is activated at 3.5 s. It is clear that the

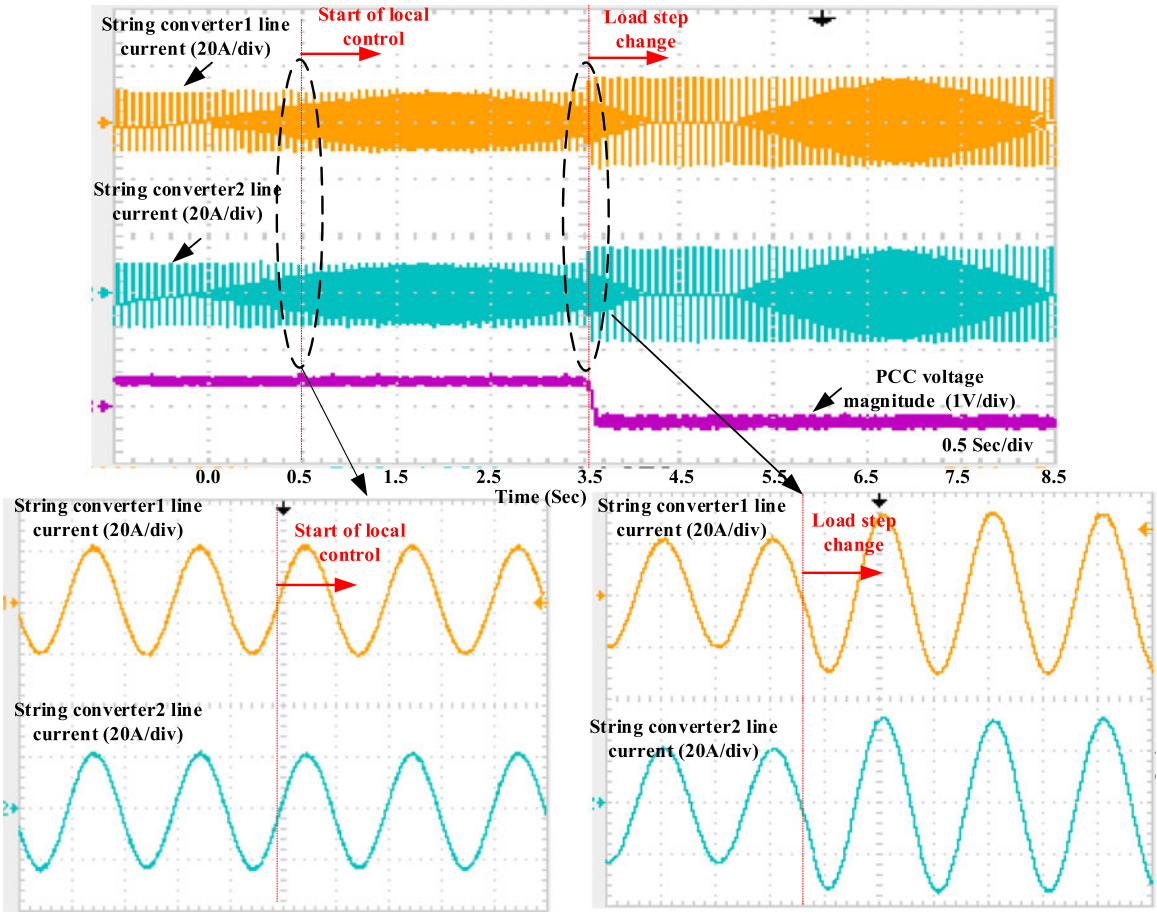

Fig. 32. Two string converters real line current and PCC voltage magnitude (*Islanding*).

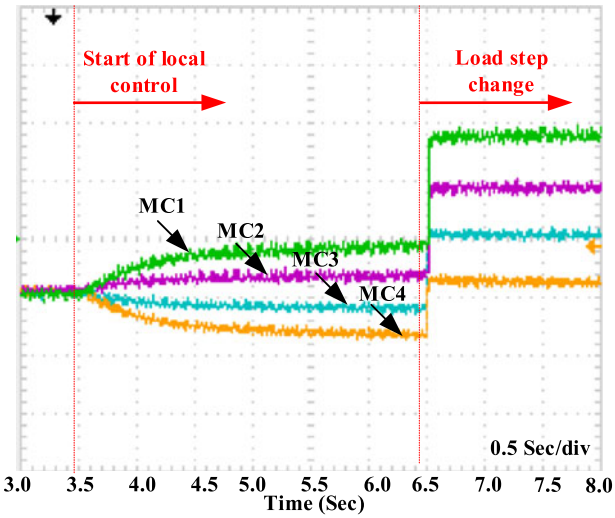

Fig. 33. Microconverters real power control performance (String converter1; *Islanding*).

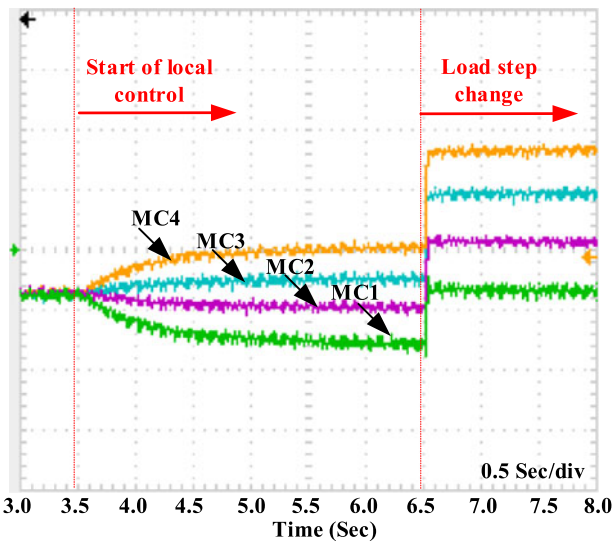

Fig. 34. Microconverters reactive power control performance (String converter1; *Islanding*).

start of local power control does not affect the output power characteristic of the string converter.

The detailed real and reactive power of each microconverter in this grid-tied system is shown in Figs. 26 and 27, respectively. In this system, the real power and reactive power ratios of microconverter1 to microconverter4 are $\varepsilon_{p,1} = 0.325$, $\varepsilon_{p,2} = 0.275$, $\varepsilon_{p,3} = 0.225$, $\varepsilon_{p,4} = 0.175$, $\varepsilon_{q,1} = 0.175$, $\varepsilon_{q,2} =$

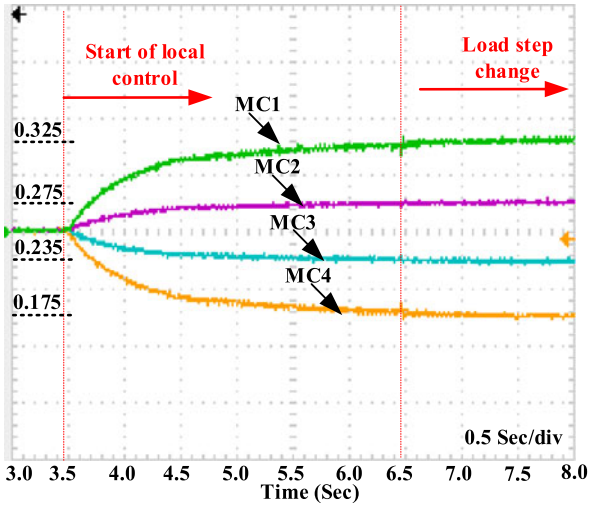

Fig. 35. Microconverters real power ratio (String converter1; *Islanding*).

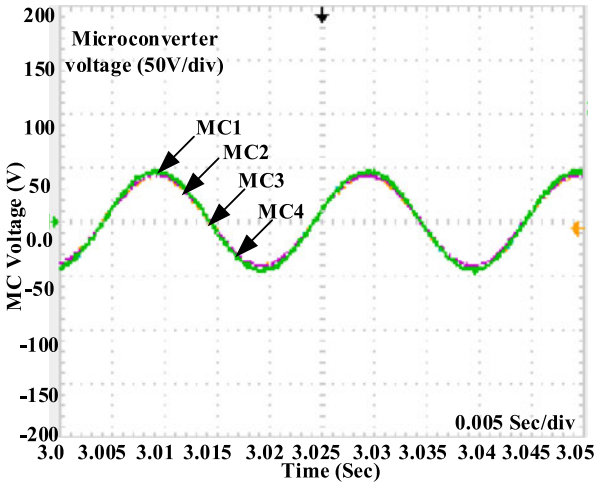

Fig. 37. Microconverters voltage waveforms before local power control (String converter1; *Islanding*).

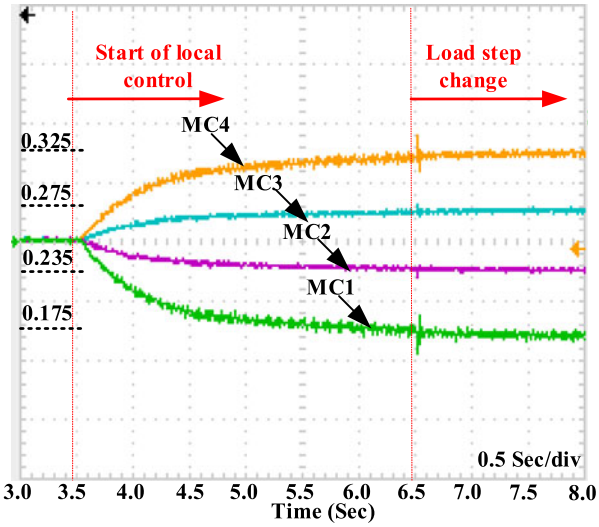

Fig. 36. Microconverters reactive power ratio (String converter1; *Islanding*).

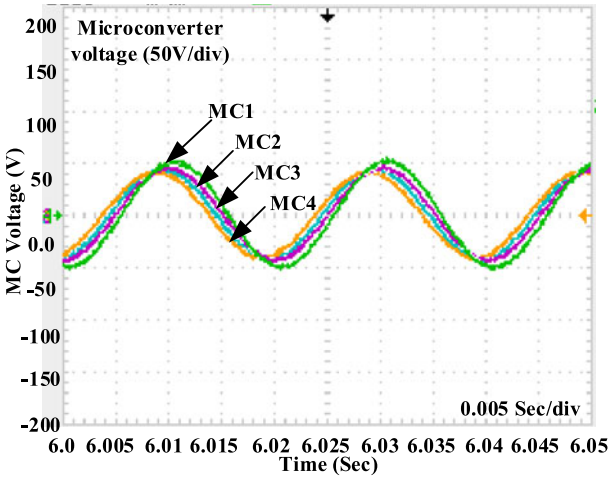

Fig. 38. Microconverters voltage waveforms after local power control (String converter1; *Islanding*).

0.225, $\varepsilon_{q,3} = 0.275$, and $\varepsilon_{q,4} = 0.325$. As shown, the output power of all microconverters reaches the reference in around 1.5 s after the start of the local power control.

The corresponding voltage waveforms of microconverters are shown in Figs. 28 and 29. Fig. 28 shows the voltage waveforms when the local power control is not activated. As all microconverters have the same reference voltage, the voltage waveforms of all microconverters are almost the same. Nevertheless, when the output powers of microconverters are different with the activation of the local power control, the microconverter voltages are different as demonstrated in Fig. 29.

2) Islanding Operation: An experimental islanding system with two string converters is tested. Each string converter is composed of four series-connected microconverters. An *RL* load bank is adopted as the PCC load.

First, the real and reactive power sharing performance of parallel string converters is investigated in Figs. 30 and 31. In this process, the local power control is activated at 0.5 s. Then, there is a PCC load step jump at 3.5 s. It can be clearly seen that the proposed method ensures an accurate sharing of real and reactive power between string converters and the performance is not affected even when the local power regulation is activated at microconverter local controllers or there is a sudden increase of PCC load demand.

The long-time scale line current performance of both string converters is shown in the upper part of Fig. 32. It can be seen that the currents of string converters have the same magnitude in the entire process.

The zoom-in current waveforms are shown in the lower part of Fig. 32. First, it can be clearly noticed from the left half that the start of local power control does not bring any obvious disturbance to the current sharing performance of string converters. Then, the right half waveforms demonstrate that the dynamic current sharing is accurate even when the PCC load has a step jump.

The power control performance of microconverters in string converter1 is illustrated in Figs. 33 and 34. First, all microconverters have the same output real and reactive power when the

local power control is disabled. When the local power control is enabled and the real power and reactive power ratios of micrconverter1 to micoconverter4 are set as $\varepsilon_{p,1} = 0.325$, $\varepsilon_{p,2} = 0.275$, $\varepsilon_{p,3} = 0.225$, $\varepsilon_{p,4} = 0.175$, $\varepsilon_{q,1} = 0.175$, $\varepsilon_{q,2} = 0.225$, $\varepsilon_{q,3} = 0.275$, and $\varepsilon_{q,4} = 0.325$, it can be seen that the output real and reactive power of microconverters slowly reach a new steady-state. Nevertheless, when there is a step jump of PCC load demand, the microconverter output power rapidly changes to the new steady-state.

Since the output power of all microconverters is measured, the output power ratios for each microconverter can be investigated accordingly. This is shown in Figs. 35 and 36. As expected, the output real power ratio and reactive power ratio are 0.25 for all microconverters, before the activation of local power control. When the local power control is enabled, the output power ratio of each converter slowly reaches the reference in around 3 s. As the output power ratio reference is fixed after the start of local power control, it is interesting to note that the curves in Figs. 35 and 36 have no obvious disturbance even when there are sudden PCC load demand disturbances.

Finally, the voltage waveforms of microconverters are shown in Figs. 37 and 38. Similar to the simulation, the voltages are almost the same without local control. When the local power control is activated in the microconverter local controller, the waveforms have magnitude and phase angle adjustments according to the output power demand. Thus, obvious voltage waveform differences can be noticed in Fig. 38.

V. Conclusion

To have better power control of distributed energy resources based microgrid, a new hybrid microgrid configuration with parallel- and series-connected LV microconverters is proposed. In this system, a few series-connected microconverters form a string converter and the power sharing between parallel string converters is realized by using droop control. Then, the controllable power distribution among series-connected microconverters is achieved by a simple feed-forward voltage compensator. To effectively coordinate the power sharing between parallel string converters and the power demand redistribution among series microconverters, an LBC system using the fundamental component of string converter line current as a synchronizer is also developed.

With the proposed hybrid microgrid configuration, the corresponding power control scheme, and the LBC system between string converter central controller and microconverter local controllers, all microconverters in the system are able to participate in the power sharing in both grid-tied and islanding microgrid operation modes in a decentralized manner.

References

[1] R. H. Lasseter, "Microgrids," in *Proc. IEEE Power Eng. Soc. Winter Meeting*, 2002, pp. 305–308.

[2] J. M. Guerrero, L. G. Vicuna, J. Matas, M. Castilla, and J. Miret, "Output impedance design of parallel-connected UPS inverters with wireless load sharing control," *IEEE Trans. Ind. Electron.*, vol. 52, no. 4, pp. 1126–1135, Aug. 2005.

[3] J. M. Guerrero, L. G. Vicuna, J. Matas, M. Castilla, and J. Miret, "A wireless controller to enhance dynamic performance of parallel inverters in distributed generation systems," *IEEE Trans. Power Electron.*, vol. 19, no. 4, pp. 1205–1213, Sep. 2004.

[4] J. He and Y. W. Li, "An enhanced microgrid load demand sharing strategy," *IEEE Trans. Power Electron.*, vol. 19, no. 5, pp. 1184–1194, May 2014.

[5] Q.-C. Zhang, "Robust droop controller for accurate proportional load sharing among inverters operated in parallel," *IEEE Trans. Ind. Electron.*, vol. 60, no. 4, pp. 1281–1290, Apr. 2013.

[6] M. Savaghebi, A. Jalilian, J. C. Vasquez, and J. M. Guerrero, "Autonomous voltage unbalance compensation in an islanded droop controlled microgrid," *IEEE Trans. Ind. Electron.*, vol. 60, no. 4, pp. 1390–1402, Apr. 2013.

[7] Q.-C. Zhong, "Harmonic droop controller to reduce the voltage harmonics of inverters," *IEEE Trans. Ind. Electron.*, vol. 60, no. 3, pp. 936–945, Mar. 2013.

[8] Z. He and Y. Xing, "Distributed control for UPS modules in parallel operation with rms voltage regulation," *IEEE Trans. Ind. Electron.*, vol. 55, no. 8, pp. 3133–3141, Aug. 2008.

[9] H. Han, Y. Liu, Y. Sun, and J. M. Guerrero, "An improved droop control strategy for reactive power sharing in islanded microgrid," *IEEE Trans. Power Electron.*, vol. 30, no. 6, pp. 3133–3141, Jun. 2015.

[10] K. D. Brabandere, B. Bolsens, J. V. D. keybus, A. Woyte, and J. Driesen, "A voltage and frequency droop control method for parallel inverters," *IEEE Trans. Power Electron.*, vol. 22, no. 4, pp. 1107–1115, Jul. 2007.

[11] Y. Li and Y. W. Li "Power management of inverter interfaced autonomous microgrid based on virtual frequency-voltage frame," *IEEE Trans. Smart Grid*, vol. 2, no. 1, pp. 30–40, Mar. 2011.

[12] J. He and Y. W. Li, "Analysis, design and implementation of virtual impedance for power electronics interfaced distributed generation," *IEEE Trans. Ind. Appl.*, vol. 47, no. 6, pp. 2525–2538, Nov./Dec. 2011.

[13] Y. Zhu, F. Zhuo, F. Wang, B. Liu, R. Gou, and Y. Zhao, "A virtual impedance optimization method for reactive power sharing in networked microgrid," *IEEE Trans. Power Electron.*, vol. 31, no. 4, pp. 2890–2904, May 2016.

[14] X. Lu, J. M. Guerrero, K. Sun, and J. C. Vasquez, "An improved droop control method for dc microgrids based on low bandwidth communication with dc bus voltage restoration and enhanced current sharing accuracy," *IEEE Trans. Power Electron.*, vol. 29, no. 4, pp. 1900–1812, Apr. 2013.

[15] J. M. Guerrero, J. C. Vasquez, J. Matas, L.G. de Vicuna, and M. Castilla, "Hierarchical control of droop-controlled ac and dc microgrids—A general approach toward standardization," *IEEE Trans. Ind. Electron.*, vol. 55, no. 1, pp. 158–172, Jan. 2011.

[16] Q. Shafiee, J. M. Guerrero, and J. C. Vasquez, "Distributed secondary control for islanded microgrids—A new approach," *IEEE Trans. Power Electron.*, vol. 29, no. 2, pp. 1018–1031, Feb. 2014.

[17] J. Liu, Y. Miura, and Y. T. Ise, "Comparison of dynamic characteristics between virtual synchronous generator and droop control in inverter-based distributed generators," *IEEE Trans. Power Electron.*, vol. 31, no. 5, pp. 3600–3611, May 2016.

[18] Q. Li and P. Wolfs, "A review of the single phase photovoltaic module integrated converter topologies with three different dc link configuration," *IEEE Trans. Power Electron.*, vol. 23, no. 3, pp. 1320–1333, May 2008.

[19] B. Xiao, L. Hang, J. Mei, C. Riley, L. M. Tolbert, and B. Ozpineci, "Modular cascaded H-bridge multi-level PV inverter with distributed MPPT for grid-connected applications," *IEEE Trans. Ind. Appl.*, vol. 51, no. 2, pp. 1722–1732, Mar./Apr. 2015.

[20] Y. Yu, G. Konstantinou, B. Hredzak, and V. G. Agelidis, "Power balance of cascaded H-bridge multilevel converters for large scale photovoltaic integration," *IEEE Trans. Power Electron.*, vol. 31, no. 1, pp. 292–303, Jan. 2016.

[21] L. Liu, H. Li, Y. Xue, and W. Liu, "Decoupled active and reactive power control for large-scale grid-connected photovoltaic systems using cascaded modular multilevel converters," *IEEE Trans. Power Electron.*, vol. 30, no. 1, pp. 176–187, Jan. 2015.

[22] H. Mahmood, D. Michaelson, and J. Jiang, "A power management strategy for PV/battery hybrid systems in islanded microgrids," *IEEE J. Emerging Sel. Topics Power Electron.*, vol. 2, no. 4, pp. 870–882, Dec. 2014.

[23] H. Mahmood, D. Michaelson, and J. Jiang, "Strategies for independent deployment and autonomous control of PV and battery units in islanded microgrids," *IEEE J. Emerging Sel. Topics Power Electron.*, vol. 3, no. 2, pp. 742–755, Sep. 2015.

[24] L. Zhang, K. Sun, Z. Huang, and Y. W. Li "A grid-tied photovoltaic generation system based on series-connected module integrated inverters with adjustable power factor," in *Proc. 2015 IEEE Energy Convers. Congr. Expo.*, Montreal, Canada, 2015, pp. 6864–6870.

[25] F. Lu, B. Choi, and D. Maksimovic, "Autonomous control of series-connected low voltage photovoltaic microinverters," in *Proc. 2015 IEEE 16th Workshop Control Model. Power Electron.*, 2015, pp. 1–6.
[26] B. Liang, Y. W. Li, J. He, and C. Wang, "A series-DG based autonomous islanding microgrid," in *Proc. IEEE Appl. Power Electron. Conf. Expo.*, 2016, pp. 1249–1252.
[27] E. Jacobsen and R. Lyons, "The sliding DFT," *IEEE Signal Process. Mag.*, vol. 20, no. 2, pp. 74–80, Mar. 2003.
[28] X. Lu, K. Sun, J. M. Guerrero, J. C. Vasquez, and L. Huang, "State-of charge balance using adaptive droop control for distributed energy storage systems in dc microgrid applications," *IEEE Trans. Ind. Electron.*, vol. 61. no. 6, pp. 2804–2815. Jun. 2014
[29] X. Lu, J. M. Guerrero, K. Sun, J. C. Vasquez, R. Teodorescu, and L. Huang, "Hierarchical control of parallel ac-dc converter interfaces for hybrid microgrids," *IEEE Trans. Smart Grid*, vol. 2, no. 2, pp. 683–692, Feb. 2014
[30] C. D. Townsend, Y. Fu, G. Konstantinou, and V. G. Agelidis, "Cascaded H-bridge multilevel PV topology for alleviation of per-phase power imbalances and reduction of second harmonic voltage ripple," *IEEE Trans. Power Electron.*, vol. 31, no. 8, pp. 5574–5586, Aug. 2014.
[31] Q.-C. Zhong, P.-L. Nguyen, Z. Ma, and W. Sheng, "Self-synchronized synchronverters: inverters without a dedicated synchronization unit," *IEEE Trans. Power Electron.*, vol. 29, no. 2, pp. 617–630, Feb. 2014.
[32] L. Asiminoaei and F. Blaabjerg, "Detection is key—Harmonic detection methods for active power filter applications," *IEEE Ind. Appl. Mag.*, vol. 13, no. 4, pp. 22–33, Jul./Aug. 2007.
[33] M. Nuotio, M. Ilic, Y. Liu, J. Bonanno, and P. J. Verlinden, "Innovative ac photovoltaic module system using series connection and universal low-voltage micro inverters," in *Proc. IEEE Photovolt. Spec. Conf.*, 2014, pp. 1367–1369.

Jinwei He (M'15) received the B.Sc. degree from Southeast University, Nanjing, China, the M.Sc. degree from the Institute of Electrical Engineering, Chinese Academy of Sciences, Beijing, China, and the Ph.D. degree from the University of Alberta, Edmonton, AB, Canada, all in electrical engineering, in 2005, 2008, and 2013, respectively.

In September 2015, he joined Tianjin University, Tianjin, China, where he is currently a Professor. His research interests include power electronics for microgrid and distributed power generation.

Yunwei Li (SM'12) received the B.Sc. (Eng.) degree in electrical engineering from Tianjin University, Tianjin, China, in 2002, and the Ph.D. degree in the area of power electronics engineering from the Nanyang Technological University, Singapore, in 2006.

In 2005, he was a Visiting Scholar with Aalborg University, Aalborg, Denmark. From 2006 to 2007, he was a Postdoctoral Research Fellow with Ryerson University, Toronto, ON, Canada. In 2007, he worked with Rockwell Automation Canada and later joined the Department of Electrical and Computer Engineering, University of Alberta, Edmonton, AB, Canada, in the same year. He is currently a Professor with the University of Alberta. His research interests include distributed generation, microgrid, renewable energy, high power converters, and electric motor drives.

Dr. Li serves as an Associate Editor for the IEEE TRANSACTIONS ON POWER ELECTRONICS and the IEEE TRANSACTIONS ON INDUSTRIAL ELECTRONICS. He also worked as a Guest Editor for the IEEE TRANSACTIONS ON INDUSTRIAL ELECTRONICS Special Session on Distributed Generation and Microgrids. He received the 2013 Richard M. Bass Outstanding Young Power Electronics Engineer Award from the IEEE Power Electronics Society.

Chengshan Wang (SM'XX) received the Ph.D. degree in electrical engineering from Tianjin University, Tianjin, China.

He is currently a Professor in the School of Electrical Engineering and Automation, Tianjin University. His research interests include distributed generation and microgrids, power distribution system analysis and planning, and power system security analysis.

Yiwei Pan was born in China, in 1993. He received the B.S. degree in automation in 2015 from the School of Control Science and Engineering, Shandong University, Ji'nan, China, where he is currently working toward the M.S. degree in power electronics.

His current research interests include multilevel converters and power electronics for microgrid.

Chenghui Zhang (M'13) was born in China, in 1963. He received the B.S. and M.S. degrees from the Shandong University of Technology, Zibo, China, in 1985 and 1988, respectively, and the Ph.D. degree from Shandong University, Jinan, China, in 2001, all in control theory and control engineering.

In 1988, he joined Shandong University, where he is currently a Full Professor in the School of Control Science and Engineering, and the Director of Research Center of Power Electronics Energy-Saving Technology and Equipment of the Chinese Education Ministry. In 2009, he was selected as a Changjiang Scholar of the Education Ministry and a Taishan Scholar of Shandong Province. His current research interests include optimal control of engineering, power electronics and motor drives, and energy-saving techniques.

Xiangyang Xing (S'14) was born in China, in 1985. He received the B.S. and M.S. degrees in control theory and control engineering from the Qufu Normal University, Ji'ning, China, in 2009 and 2012, respectively. He is currently working toward the Ph.D. degree in the School of Control Science and Engineering, Shandong University, Ji'nan, China.

His current research interests include multilevel converters, power conversion, and renewable power generation.